MLM-2752

Surface Studies on the Thermite Mixture of Al/Cu_2O. II. Thickness Measurements of Carbon and of Aluminum Oxide on Aluminum, and Changes in Copper Chemistry

Alessandro Rengan, Lowell D. Haws,
William E. Moddeman and Pu Sen Wang

October 10, 1980

Monsanto

MOUND FACILITY
Miamisburg, Ohio 45342

operated by
MONSANTO RESEARCH CORPORATION
a subsidiary of Monsanto Company

for the
U. S. DEPARTMENT OF ENERGY

Contract No. DE-AC04-76-DP00053

NOTICE

Printed in the United States of America
Available from
National Technical Information Service
U. S. Department of Commerce
5285 Port Royal Road
Springfield, VA 22161

NTIS price codes
Printed copy: A03
Microfiche copy: A01

MLM-2752
UC-4

Surface Studies on the Thermite Mixture of Al/Cu_2O. II. Thickness Measurements of Carbon and of Aluminum Oxide on Aluminum, and Changes in Copper Chemistry

Alessandro Rengan*, Lowell D. Haws,

William E. Moddeman and Pu Sen Wang

Issued: October 10, 1980

★Graduate Student, University of Dayton

MOUND FACILITY
Miamisburg, Ohio 45342

operated by
MONSANTO RESEARCH CORPORATION
a subsidiary of Monsanto Company

for the
U. S. DEPARTMENT OF ENERGY

Contract No. DE-AC04-76-DP00053

Contents

Abstract

Improved surface analysis techniques of x-ray induced photoelectron spectroscopy (XPS) and high resolution Auger spectroscopy (AES) were used to study thermite materials. The thermite under examination was a powdered mixture of aluminum metal and cuprous oxide in a mole ratio of 2/3. These improved techniques were used to examine the surfaces of the aluminum metal and of the cuprous oxide for the presence, the amount, and the thickness of contaminants. Carbon, aluminum oxide, cupric oxide, and metallic-like copper were found on the reactants and mixtures. XPS and AES spectra of aluminum and copper are given, and equations are derived which allow for the calculation of carbon and oxide thicknesses.

1. Carbon and oxide thickness

1.1. General equations

X-ray photoelectron spectroscopy (XPS) is a surface-sensitive technique that can be used to obtain thickness values of thin films on the very sensitive monolayer level of coverage. The maximum depth of analysis with XPS is dependent on the mean free path of inelastically scattered photoelectrons through the solid. In the following discussion, the general equations that are used to obtain thickness information in XPS are developed. These equations will be used in the following sections to calculate the carbon and/or oxide film thicknesses on the thermite reactants, aluminum and Cu_2O.

The mean free path of a photon-excited electron increases with kinetic energy [1]. Thus, in XPS the analyzed depth is dependent on the energy of the incident radiation. For example, the analyzed depth of an aluminum photoelectron is less when excited by Mg K_α x-rays of 1254 eV than when excited by Si K_α x-rays of 1739 eV. Si K_α x-rays were used in this Al/Cu_2O thermite study. There are advantages in using x-rays emitted from a silicon anode in studying Al/Cu_2O thermite materials. A detailed discussion of these advantages and a detailed introduction to x-ray photoelectron spectroscopy were discussed in a previous report [2]. High resolution Auger electron spectroscopy was also used in this study. The Auger process and the processing of Auger data are also discussed.

The nearly free electron nature of aluminum metal shows a high affinity for atmospheric oxygen with the subsequent formation of an aluminum oxide layer. Surface examinations of the ambient oxide layer formed on aluminum metal have been measured and have been shown to vary from a few angstrom to $\sim$25Å thick [3].

It is evident from this present study that a surface-sensitive technique like XPS can provide valuable information on film thicknesses in thermite materials.

The intensity of electrons of a given energy in a homogeneous material can be expressed by the following relationship [4]:

$$dI = F\alpha A\kappa n \exp(-x/\lambda)$$

where F is the photon flux; α is the cross section for photoionization; A is the sample area from which the photoelectrons are detected; κ is the spectrometer transmission factor; n is the number of atoms of the element per cm^3; and λ is the mean free path of the photoelectron. The mean free path is dependent on (a) the kinetic energy of the photoelectron and (b) the nature of the sample medium through which the photoelectron passes. x is the distance through the material that the inelastically scattered photoelectron must travel.

For a layer of "infinite" thickness, the total intensity is obtained by integrating from $o< x <\infty$;

$$\int_o^{\infty} dI = \int_o^{\infty} F\alpha A\kappa n \cdot \exp(-x/\lambda)dx \qquad (1)$$

or

$$I^* = F\alpha A\kappa n\lambda$$

for an ideal homogeneous medium.

In this study, the layer or layers of interest were of finite thickness. The aluminum was found to be contaminated with an oxide film and a carbonaceous film. Figure 1 represents a layered system of metal/metal oxide/carbon, which we will use to develop the equation to calculate to the oxide thickness on aluminum.

Consider a carbon photoelectron, e_C, from a depth x where $0 <x <d_C$. The total carbon intensity from this finite layer is:

$$I_C = \int_o^{d_C} F\alpha A\kappa n_C \exp(-x/\lambda_C)dx$$

or

$$I_C = F\alpha A\kappa n_C\lambda_C [1-\exp(d_C/\lambda_C].$$

Combining with Eq. (1) gives:

$$I_C = I_C^* [1-\exp(-d_C/\lambda C)] \qquad (2)$$

Next, consider an aluminum electron from the oxide layer, e_O, at a depth x below the surface, where d_C x d_O. The total aluminum intensity from the oxide layer is:

$$I_O = \int_{d_C}^{d_C + d_O} F\alpha A\kappa n_O [\exp-(x-d_C)/\lambda_O] \; [\exp-d_C/(\lambda_O)_C]dx$$

or

$$I_O = F\alpha A\kappa n_O\lambda_O [\exp-d_C/(\lambda_O)_C] \; [1-\exp-d_O/\lambda_O] \qquad (3)$$

where $(\lambda_O)_C$ is the mean free path of the aluminum electrons of aluminum oxide through a finite carbon layer, d_C.

Finally, consider an aluminum electron, e_M, emanating at a depth x from the surface of a metal, where $d_C + d_O <x <\infty$. Then the total aluminum intensity from aluminum metal is:

$$I_{Al} = \int_{d_C+d_O}^{\infty} F\alpha A\kappa n_M [\exp(x-d_C-d_O)/\lambda_M] \; [\exp-d_O/(\lambda_M)_O][\exp-d_C/(\lambda_M)C]dx$$

or

$$I_{Al} = I_M^* [\exp-d_O/(\lambda_M)_O][\exp-d_C/(\lambda_M)_C] \qquad (4)$$

where $(\lambda_M)_O$ and $(\lambda_M)_C$ are the mean free paths of aluminum electrons through the oxide and carbon layers, respectively. Equations have now been established relating an experimentally measurable intensity I to oxide thickness 'd_O'.

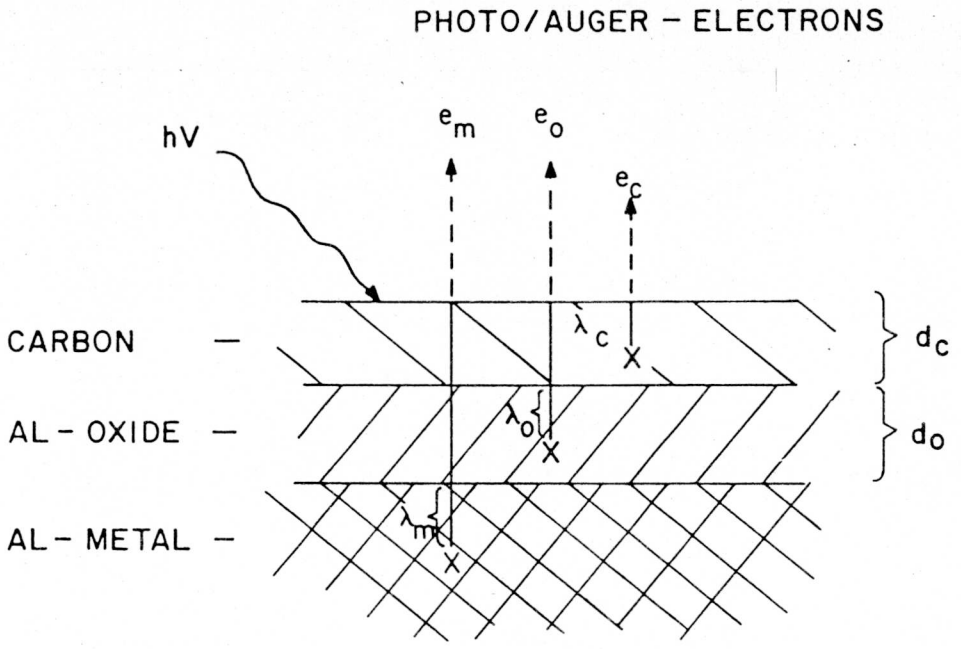

d_c — DEPTH OF CARBON LAYER

d_o — DEPTH OF OXIDE LAYER

λ_m — MEAN FREE BATH OF $\mathring{A}L$ ELECTRON THROUGH ALUMINUM

λ_o — MEAN FREE PATH OF AL^{+++} ELECTRONS THROUGH THE OXIDE

λ_c — MEAN FREE PATH OF CARBON ELECTRONS

FIGURE 1 - Representation of the analysis depth and the mean free path in photoelectron and high resolution Auger spectroscopy for a three-layered system.

The unknowns in Eqs. (2), (3), and (4) are:

(1) the various mean free paths: λ_C, $(\lambda_O)_C$, $(\lambda_M)_C$, λ_O, $(\lambda_M)_O$;

(2) the intensity of the homogeneous material of infinite I_C^*, I_O^*, I_M^*; and

(3) the oxide and carbon thicknesses to be determined, d_O and d_C.

1.2. Determination of the various mean free paths

To determine values for the mean free path of electrons through various materials requires time beyond the present thrust of this research effort; hence, literature values were used. As was previously stated, the mean free path of a photoelectron is dependent on its kinetic energy and the material through which it passes. Battye et al. [5] studied the attenuation of photoelectrons by aluminum oxide of kinetic energies from 157 eV to 1404 eV. The data of Battye were previously fitted to a quadratic regression model [2]. Table I summarizes the mean free path values extracted from the regression model. To calculate the mean free path for 1616 eV, the quadratic had to be extended beyond the available data.

Henke [6] showed that attenuation lengths in stearic acid multilayers are 60Å and 90Å for 750 eV and 1350 eV electrons, respectively. Alternately, Wagner [1] showed that the mean free path of a photoelectron is exponentially related to the kinetic energy, E, by the simple relationship:

$$\lambda = kE^p \qquad (5)$$

where k and p are constants to be determined. Substitution of Henke's values into Eq. (5) gives k = 0.624 and p = 0.69. Hence, $\lambda = 0.624\ E^{0.69}$. Substitution of the energies for the aluminum K-LL Auger, the aluminum 2s, and the carbon 1s photoelectrons excited by Si K_α x-rays into Eq. (5) allows for the calculation of mean free paths. These calculations are also summarized in Table 1.

1.3. Intensity determination from an infinite homogeneous material

The intensities of Auger lines and of photopeaks were measured from clean homogeneous substrates of the three materials, carbon, aluminum oxide, and aluminum metal. In these studies it was essential to minimize the number of variables associated with Eq. (1). Photon flux, F, was kept constant by means of a highly stabilized supply. Area of the sample, A, was kept to 5 x 5 mm^2, except when noted. A change in sample dimension to 5 x 6 mm^2 showed a vast difference in intensity values. This will be discussed later. The photoelectron cross section, α, and the man free path, λ, are constant for a particular energy level and element. The instrumental transmission function, k, remained constant during the entire study. Thus, $I^* \propto n$, the number of atoms of an element per cm^3.

1.3.1. Carbon, I_C^* High molecular weight carbon containing compounds layered on a 5 x 5 mm^2 aluminum foil were used to measure I^* for carbon. Candle wax, Apiezon grease, stearic acid, and diffusion pump oil were the carbon-containing materials used. The values for I^* are given in Table 2. Proof of "infinite" thickness was obtained by scanning over

Table 1 - MEAN FREE PATH VALUES IN ANGSTROMS FOR THE ALUMINUM $K\text{-}L_{2,3}L_{2,3}$ AUGER, AND FOR THE ALUMINUM 2s AND CARBON 1s PHOTOELECTRONS

	Al K-LL		Al 2s		
	For Oxide of 1385 eV	For Metal of 1393 eV	For Oxide of 1615 eV	For Metal of 1618 eV	C 1s of 1454 eV
λ_C					94.9
$(\lambda_O)_C$	91.8		102.0		
$(\lambda_M)_C$		92.2		102.2	
λ_O	16.6		18.1		
$(\lambda_M)_O$		16.6		18.1	

λ_C is the mean free path of a carbon 1s photoelectron through a homogeneous carbon substance.

$(\lambda_O)_C$ is the mean free path of a photoelectron or Auger electron from aluminum of aluminum oxide through a homogeneous carbon film.

$(\lambda_M)_C$ is the mean free path of an aluminum metal photoelectron or Auger electron through a homogeneous carbon film.

λ_O is the mean free path of an aluminum oxide photoelectron or Auger electron through the oxide material itself.

$(\lambda_M)_O$ is the mean free path of an aluminum metal photoelectron or Auger electron through a homogeneous oxide layer.

Table 2 - MAXIMUM INTENSITIES, I_C^*, OBSERVED FOR INFINITELY THICK HOMOGENEOUS CARBONACEOUS FILMS

Carboneous Films (5 x 5 mm)	I_C^{*a} (counts-eV/sec)	Average (counts-eV/sec)
(1) Diffusion Pump Oil	1088, 1091, 1080	1086
(2) Candle Wax	800, 782, 803	795
(3) Apiezon Grease	823, 820, 821	821
(4) Stearic Acid	863, 876, 832	857
Average of Twelve Runs		890

[a] counts-eV/sec is a triangular approximation to the area under a photoelectron or Auger peak. The photo or Auger peak height is measured in centimeters, converted to counts per second, and then multiplied by the full-width at half maximum in electron volts.

the K-LL Auger aluminum lines with no observance of signal. A typical carbon 1s spectrum of stearic acid is represented in Figure 2 (spectrum a). A very similar carbon 1s spectrum was observed for the carbon film on the aluminum metal flakes used as the starting material in the manufacture of the thermite mixture. This is also shown in Figure 2 (spectrum b).

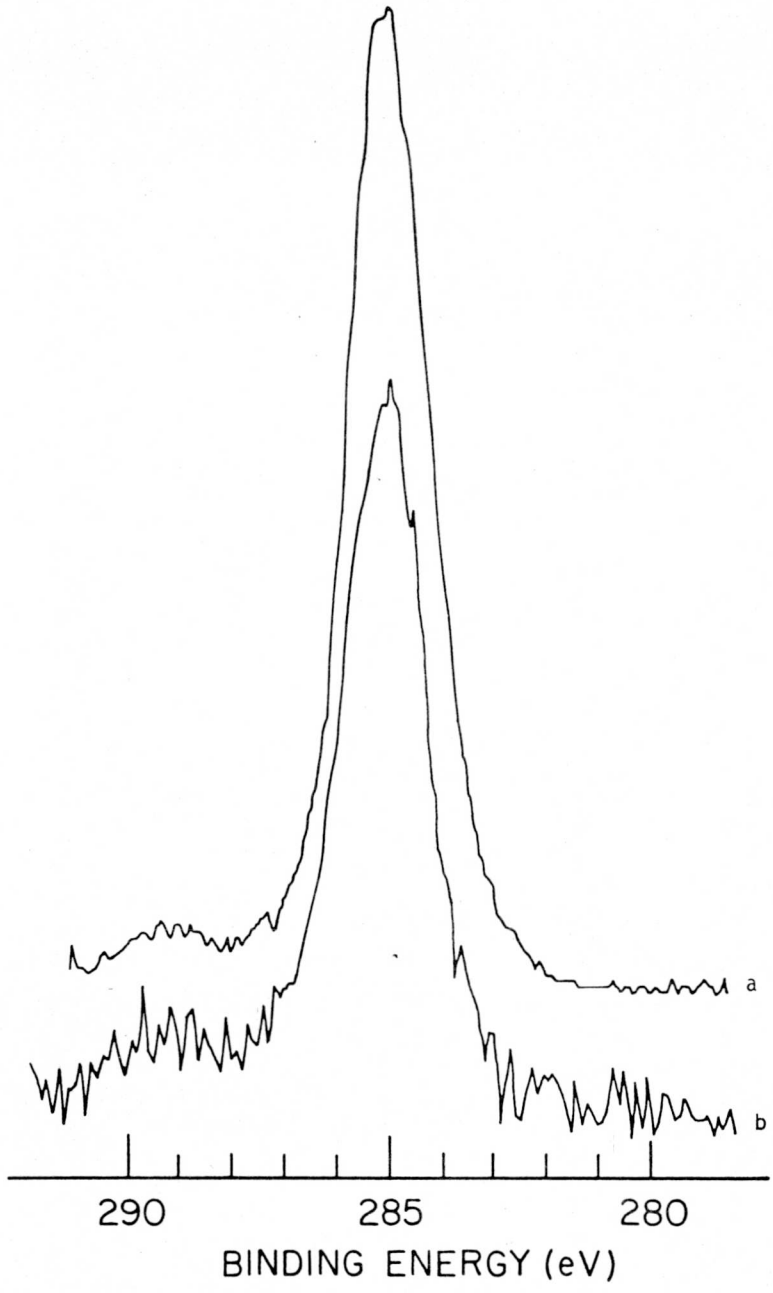

FIGURE 2 - Carbon 1s photoelectron spectra of (a) stearic acid and (b) carbon found on the aluminum flakes. The spectra were excited by Si K_{α} radiation.

1.3.2. Aluminum Oxide, I_O^* Aluminum oxide foils were prepared in a furnace preheated to ~400°C. Several 5 x 5 mm^2 aluminum foil specimens were placed in the furnace for ~12 hr. This was sufficient time to completely convert the aluminum surface to an oxide. As expected, no aluminum metal photoelectron or Auger lines were observed. Figures 3 and 4 illustrate the 1s and 2s photoelectron spectra and the K-LL Auger spectrum from aluminum of aluminum oxide.

In addition to oxide photopeaks, a small carbon photoline was measured. A correction was made for the carbon attenuation of the aluminum oxide electrons by using Eq. (2) and (3). Table 3 summarizes the measured I_O values including the corrections made for carbon contamination.

Also included in Table 3 are the I_O measured intensities for oxidized 5 x 6 mm^2 aluminum foils. As can be seen from the data in Table 3, it is imperative to keep the sample size constant in all I^* determinations.

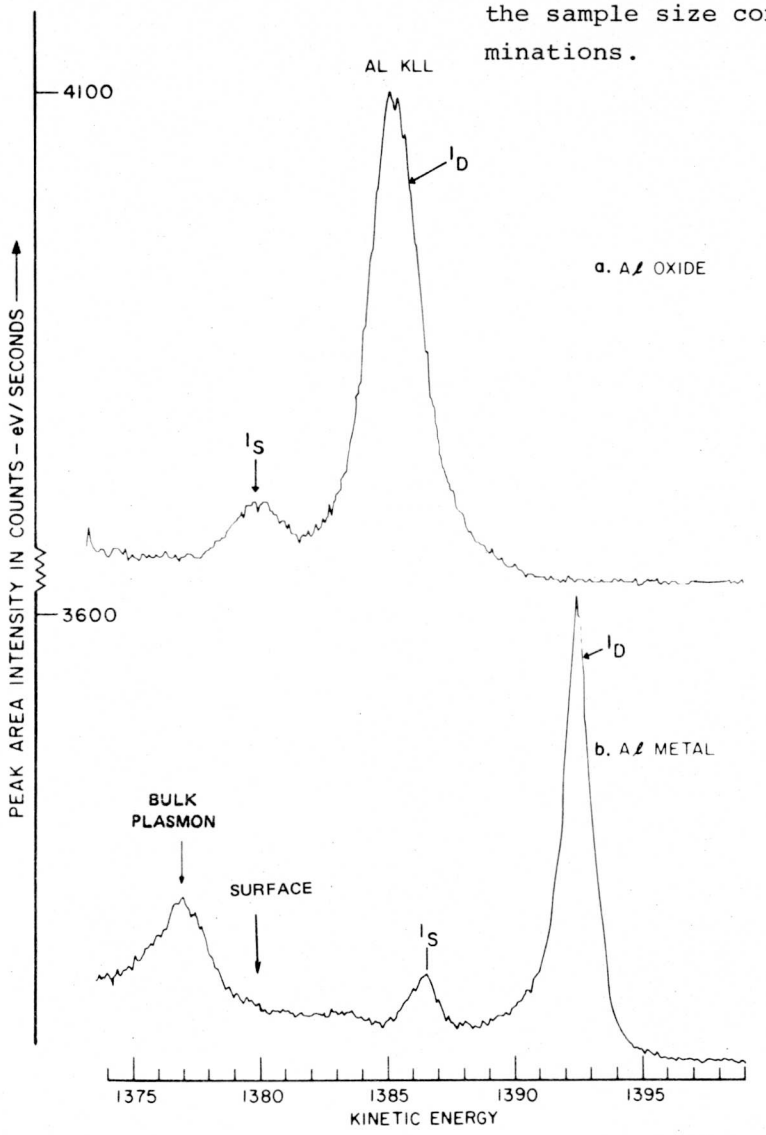

FIGURE 3 - Aluminum K-$L_{2,3}L_{2,3}$ high resolution scans for: (a) aluminum oxide and (b) aluminum metal. The strongest Auger lines, at 1392 eV for the metal and 1385.5 eV for the oxide, are the result of a $1s^1 2s^2 2p^6(^2S) \rightarrow 1s^2 2s^2 2p^4(^1D)$ transition. The lines at 1386.5 eV for the metal and 1380 eV for the oxide are the result of a $1s^1 2s^2 2p^6(^2S) \rightarrow 1s^2 2s^2 2p^4(^1S)$ transition.

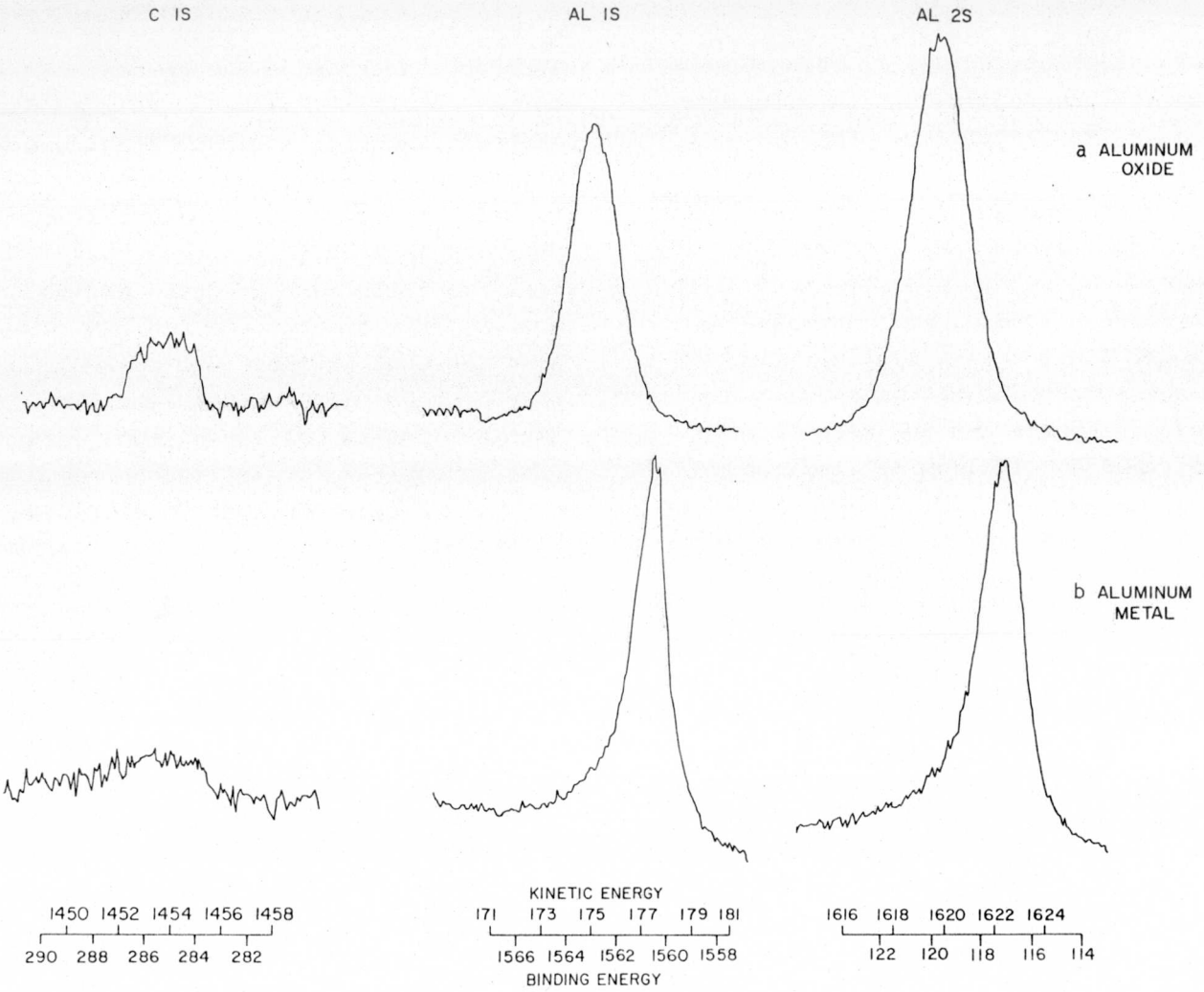

FIGURE 4 - Carbon 1s, aluminum 1s, and aluminum 2s, photoelectron spectra observed from (a) an aluminum oxide surface and (b) an aluminum surface freshly cleaned by argon ion sputtering. Chamber pressure 1 x 10^{-8} torr.

Table 3 - MAXIMUM INTENSITY, I_O^*, OBSERVED FOR INFINITELY THICK HOMOGENEOUS ALUMINUM OXIDE FILMS

Run No.	Sample Size (mm x mm)	$I_O\left(\frac{\text{counts-eV}}{\text{sec}}\right)$ Al 1s	Al K-LL	Al 2s	$I_C\left(\frac{\text{counts-eV}}{\text{sec}}\right)$ C 1s	x_c (Å)	$I_O^*\left(\frac{\text{counts-eV}}{\text{sec}}\right)$ Al 1s	Al K-LL	Al 2s
80811-1	5 x 5	--	4243	455	230	28	--	5784	601
80814-1	5 x 5	1939	4456	477	208	25	6007	5865	612
80817-1	5 x 5	1091	4291	439	292	38	6084	6477	637
80825-1	5 x 5	1614	3748	388	247	31	6559	5249	525
80828-1	5 x 5	1074	3630	361	265	33	5472	5233	508
(Average)	(5 x 5)						(6030)	(5722)	(576)
80824-1[a]	5 x 6	2581	5418	530	208				
80817-9	5 x 6	2138	5801	593	323				

[a] Bent sample.

1.3.3. Aluminum Metal, I_M^* The intensity from a homogeneous aluminum surface was determined by removing the surface contaminants of carbon and oxide with an inert argon ion beam, thus preparing a 'clean' aluminum metal substrate. Base pressure of our system was ~1 x 10^{-8} torr. Argon was let in through a leak valve to a pressure of 5 x 10^{-5} torr. After ~10 min of sputtering, it was possible to remove the metal oxide. A 3 keV, 25 mA, rastered argon ion beam was used for sample sputtering. Representative scans of the 1s and 2s photoelectrons and of the K-$L_{2,3}L_{2,3}$ Auger lines for aluminum metal following argon ion cleaning are displayed in Figures 3 and 4.

In order to calculate I_M^*, experiments were conducted in two stages. First, the regrowth rate of the oxide was determined on a freshly prepared, clean metal surface. This was done by scanning over the aluminum 1s photopeak immediately following an ion etching. This peak is extremely surface sensitive because of its low kinetic energy (176 eV). The mean free path, calculated from the method discussed previously [2], was 7.6Å. The rate of aluminum oxide regrowth as a function of time after sputtering is plotted in Figure 5. The rate of buildup of oxide is initially fast, gradually leveling off at about 3,600 sec. The limiting oxide thickness is 4Å.* The major components in the vacuum system at 1 x 10^{-8}

* Assuming that I_O^*/I_M^* is 0.63 for Al 1s photoelectrons, one can calculate a maximum oxide thickness of 4Å formed from within the vacuum system. This calculation was performed using Eqs. (2) and (3). For more details, see the section on oxide thickness calculations.

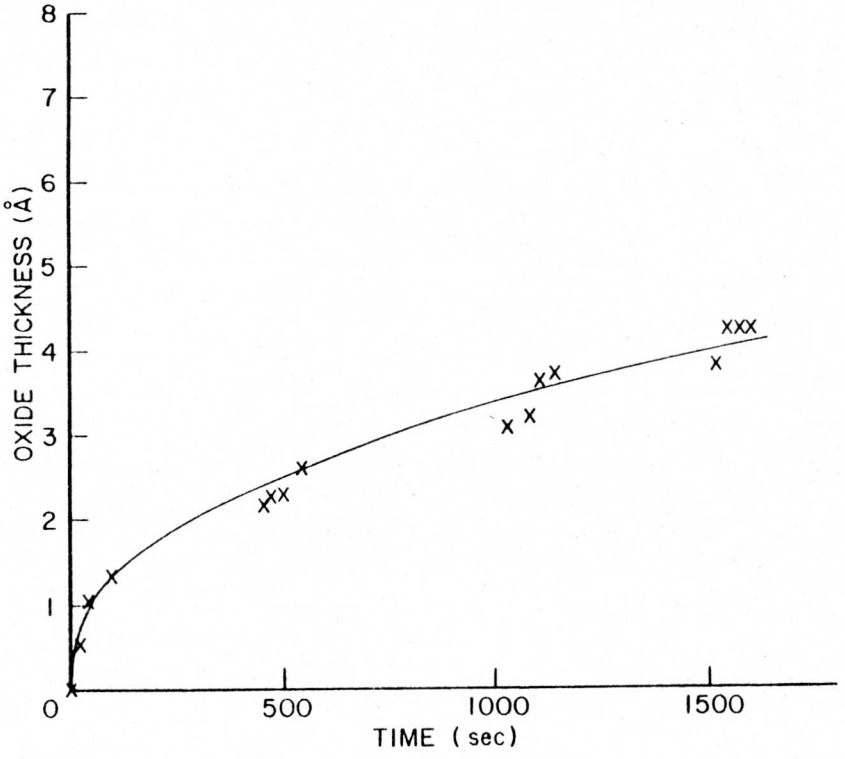

FIGURE 5 - Residual vacuum regrowth rate of surface oxide on a freshly cleaned, argon-ion-sputtered aluminum surface after sputtering for 10 min. Pressure in chamber ~1 x 10^{-8} torr.

torr are H_2, CO, and H_2O as measured with a residual gas analyzer.

The second stage was to determine the I_M^* for the K-$L_{2,3}L_{2,3}$ Auger line and the 2s photoelectron for the metal. This was accomplished by the sample sputtering and scanning sequence as discussed before. Sample sputtering was performed for 10 min, followed immediately by scans until 5,000 counts in the peak were achieved. In order to produce these sufficient counts in peak height for the Al 1s, Al K-$L_{2,3}L_{2,3}$, and the Al 2s, it required counting times of 300, 550 and 3,600 sec, respectively.

Both the aluminum K-LL from the oxide and from the metal peaks have two Auger diagram lines which are separated by 6 eV. These lines are the result of different $2p^4$ final states. In addition, the aluminum metal has a surface and bulk plasmon structure in the spectra. This plasmon structure is not found in photoelectron or Auger transitions in the oxide. Bulk plasmon losses occur as a result of a collective excitation of valence electrons occurring during photoionization of core levels. These are observable at ~15 eV from the main photoionization or Auger lines and are illustrated in Figure 3.

According to the work of Flodstrom et al. [7], the broad nature of the photoelectron peaks observed in an aluminum oxide surface is an unresolved doublet. The doublet peaks are separated by 0.9 eV with the individual lines occuring at 1.5 eV and 2.6 eV higher binding energy than aluminum metal. This doublet, according to Flodstrom, can be attributed to different chemical forms of aluminum atoms which are bound to oxygen, such as Al-O or Al-OH.

In the results to be discussed in the next section, the metal peak was simply deconvoluted with the remaining area considered as oxide. No attempt was made to distinguish between the different Al-O forms. I_M^* values for the metal were obtained by Eq. (2), (3), and (4). These values are summarized in Table 4.

1.4. Thickness calculations

1.4.1. Aluminum Oxide Samples of aluminum powder were stored at various temperatures, for different periods of time, and in two environments (dry air and argon). The samples were aged at two temperatures, ambient and 180°C, for 40, 91, and 136 days.

The sample was prepared for analysis by removing a small quantity from a glass tube containing the required sample and lightly pressing (with finger pressure) it between two pieces of 5 x 5 mm^2 indium foil. The powders adhered well to the foil so that a uniform coverage was formed. As will be seen in the discussion to follow, the sample dimension or x-ray flux need not be held constant; however, during the analysis of each powder, variations in parameters were held to a minimum.

It is possible to eliminate unwanted quantities and to solve for d_O, the oxide thickness, by taking the ratio of the Eq. (3) and (4). I_O/I_M can be written as follows:

$$\frac{I_O}{I_M} = \frac{I_O^*}{I_M^*} \frac{[\exp -d_C/(\lambda_O)_C][1 - \exp -d_O/\lambda_O]}{[\exp -d_C/(\lambda_M)_C][\exp -d_O/(\lambda_M)_O]} \quad (6)$$

If it is assumed that the mean free path of the aluminum oxide electron through the carbon layer is the same as the mean free path of the aluminum metal electron through the

Table 4 - MAXIMUM INTENSITY, I_M^*, OBSERVED FOR ALUMINUM METAL SUBSTRATE[a]

Run No.	Level or Transition	I_M	I_C	X_C (Å)	I_O	X_O (Å)	I_M^* Al 1s	I_M^* Al K-LL	I_M^* Al 2s
080710-04	1s	3500	139	16	356	1.3	8,640		
080710-06	K-LL	3400	155	18	136	0.5		4,270	
080710-08	2s	371	136	15	56	2.2			482
080711-03	1s	4670	117	13	529	1.8	10,460		
080711-05	K-LL	3700	125	14	114	0.4		4,420	
080711-09	2s	404	111	12	43	1.6			500
080712-01	1s	4310	101	11	686	2.2	9,610		
080712-03	K-LL	3630	102	11	112	0.4		4,210	
080712-05	2s	422	94	10	52	1.9			520
(Average)							(9,570)	(4,300)	(501)

[a]Intensity values, I, are given in counts-eV/sec. All samples were 5 x 5 mm^2 squares. Pressure in the chamber was ~2 x 10^{-8} torr.

the carbon layer, one can reduce Eq. (6). The error in oxide calculation from this assumption can be ignored. From the data given in Table 1 for λ, it can be shown for both the Al K-LL and Al 2s transitions:

$$\exp\left(\frac{1}{(\lambda_M)_C} - \frac{1}{(\lambda_O)_C}\right)$$

$$= \exp(-0.00005) = 1.$$

Therefore, the exponential dependence on the carbon layer can be neglected, and the assumption of $(\lambda_O)_C = (\lambda_M)_C$ is valid.

Also the assumption that the mean free path of the oxide, (λ_O), is the same as the mean free path of the metal electron through the oxide, $(\lambda_M)_O$, simplifies Eq. (6) further:

$$\frac{I_O}{I_M} = \frac{I_O^*}{I_M^*} \frac{[1-\exp -d_O/\lambda_O]}{[\exp -d_O/\lambda_O]}$$

with the only unknown being d_O. Rewriting gives

$$d_O = \lambda_O \ln\left[\frac{I_O}{I_M}\frac{I_M^*}{I_O^*} + 1\right] \qquad (7)$$

where I_O and I_M are measurable values from the XPS spectra.

Figures 6 and 7 illustrate representative scans of the aluminum powder stored for aging studies in dry air and in argon, respectively. Table 5 summarizes the measured values of the intensities, I_O I_M, for the K-$L_{2,3}L_{2,3}$ Auger transition and for the 2s photoelectron peaks. Oxide thicknesses, d_O, were calculated by means of Eq. (7). Table 5 also summarizes these calculated oxide thicknesses for each of the measured samples. The thicknesses ascertained with the K-$L_{2,3}L_{2,3}$ agree to <1.5Å of those values measured when the 2s photoelectron data are used.

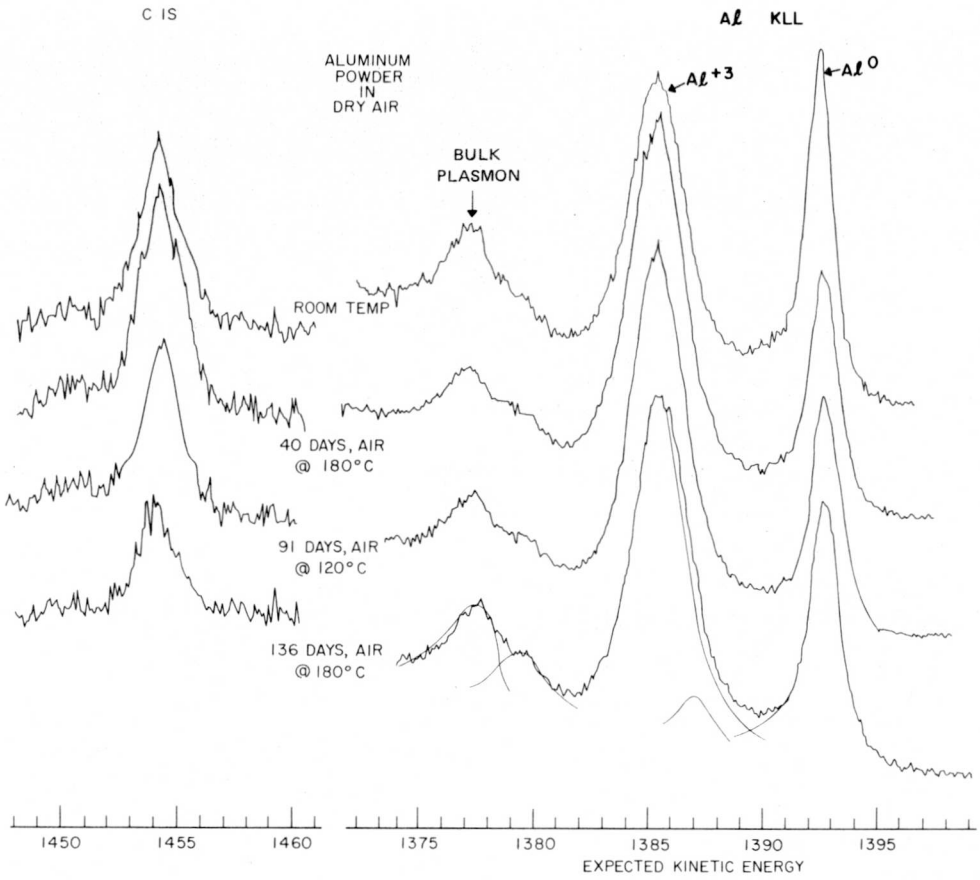

FIGURE 6 - Representative scans of carbon 1s, aluminum K-$L_{2,3}L_{2,3}$ Auger transition, and the aluminum 2s peaks for aged aluminum powders in dry air at different temperatures. Auger and photoelectron lines were excited by Si Kα radiation.

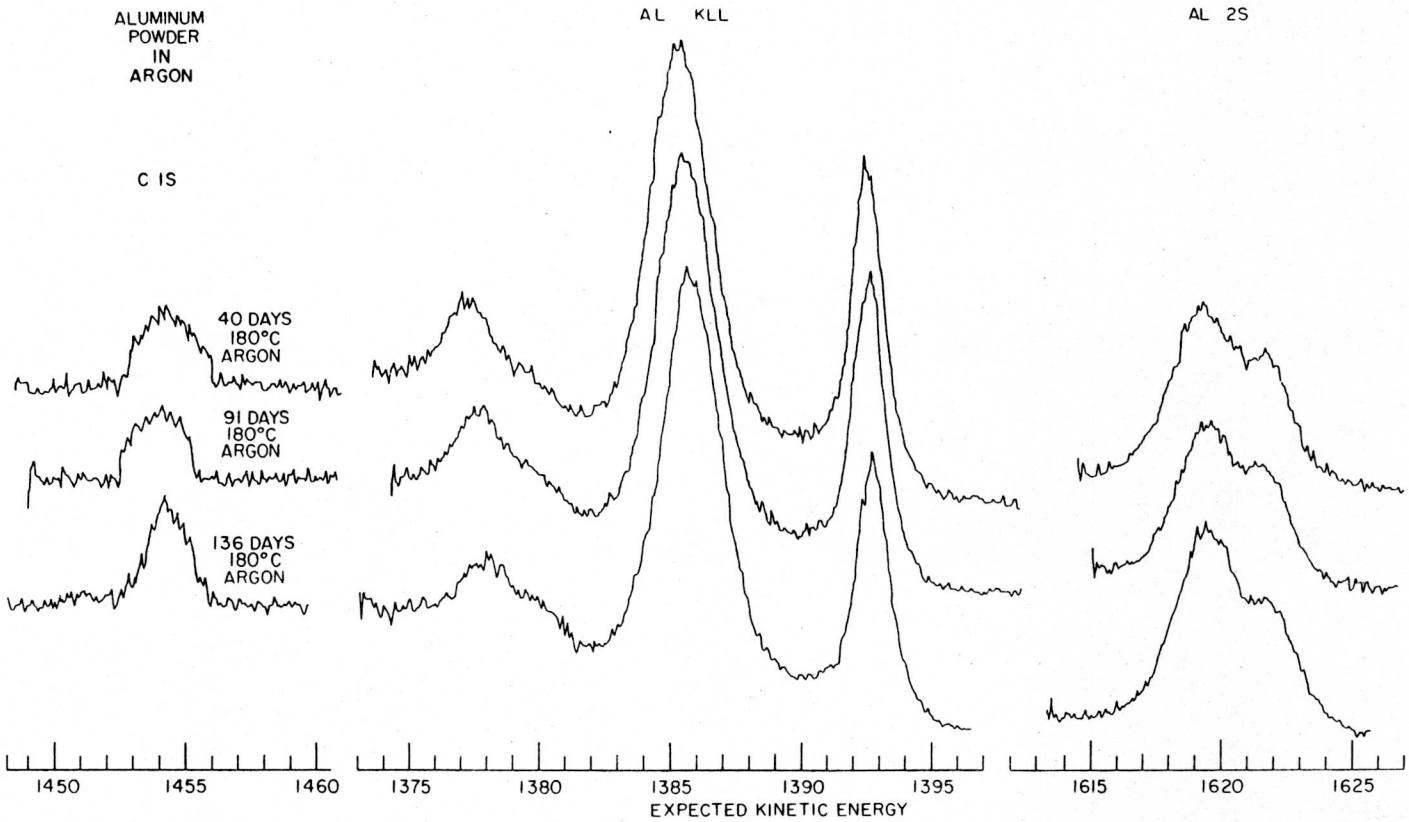

FIGURE 7 - Representative scans of carbon 1s, aluminum K-$L_{2,3}L_{2,3}$ Auger transition, and the aluminum 2s peaks for aged aluminum powders in argon at different temperatures. Auger and photoelectron lines were excited by Si K_{α} radiation.

Table 5 - SUMMARY OF OXIDE THICKNESSES MEASURED ON AGED ALUMINUM POWDERS

Sample	Run No.	Intensities[a] Measured from Aluminum $K\text{-}L_{2,3}L_{2,3}$ Auger Trans. (I_O) K-LL	Intensities[a] Measured from Aluminum (I_M) K-LL	Intensities[a] Measured from Aluminum 2s Photopeak (I_O) 2s	Intensities[a] Measured from Aluminum 2s Photopeak (I_M) 2s	Calculated Oxide Thickness in (Å) d_O from K-LL	Calculated Oxide Thickness in (Å) d_O from 2s
Air							
Room Temp.	080525-1	1403	930	105	74	8.9	10.2
Room Temp.	080525-6	1834	1158	328	228	9.2	10.5
Room Temp.	080829-1	1503	998	181	118	8.8	10.9
40 days 180°C	080530-1	1735	675	426	199	12.6	13.5
40 days 180°C	080601-1	2146	808	530	236	12.8	13.9
91 days 180°C	080526-1	2065	775	441	202	12.9	13.6
91 days 180°C	080531-1	1820	673	505	225	13.0	13.9
136 days 180°C	080712-1	847	315	192	92	12.9	13.3
136 days 180°C	080713-1	732	325	164	84	12.6	13.8
Argon							
40 days 180°C	080801-1	726	315	87	46	11.8	12.5
91 days 180°C	080803-1	678	286	72	38	12.0	12.5
136 days 180°C	080802-1	1837	769	206	103	12.0	13.0
136 days 180°C	080802-6	1106	417	93	44	12.8	13.4

[a]Intensity values are given in counts-eV/sec. All samples were finger pressed on a 5 x 5 mm^2 indium foil.

Sources of error in measuring oxide thickness are given by the variables of Eq. (1) and (7). These will be discussed in some detail at the end of this section.

1.4.2. Carbon The carbon thickness measurements were obtained in a manner similar to the oxide measurements. The carbon 1s photopeaks were scanned until a sufficient number of counts were obtained. Dividing Eq. (2) by Eq. (3) gives:

$$\left(I_C/I_O\right)\left(I_O^*/I_C\right)[1-\exp(-d_O/X_O)] = \exp[(d_C/\lambda_O)_C] - \exp[-d_C(1/\lambda_C - 1/\lambda_O)]$$

where again

$$[(1/\lambda_C) - (1/\lambda_O)] \cong 0$$

Taking the logrithm of both sides gives

$$d_C = (\lambda_O)_C \ln\left[(I_C/I_O)\ (I_C^*/I_C^*)\ [1-\exp(-d_O/\lambda_O)] + 1\right] \quad (8)$$

Note, a similar expression can be written by dividing Eq. (2) by Eq. (4). This result is given in Eq. (9).

$$d_C = (\lambda_M)_C \ln\left[(I_C/I_M)\ (I_M^*/I_C^*)\ \exp(-d_O/\lambda_O)\right] + 1 \quad (9)$$

where d_O values are obtained from Eq. (7). Peak area intensities obtained from the aluminum oxide Auger and photolines are used to calculate d_C values from Eq. (8), whereas intensities from metal lines are used in obtaining d_C values from Eq. (9). The d_C calculations are summarized in Table 6.

Table 6 - SUMMARY OF CARBON THICKNESSES MEASURED ON AGED ALUMINUM POWDERED SPECIMENS

Sample	Run No.	I_C (counts-eV/sec)	d_C From Al K-LL (Å)	d_C From Al 2s (Å)
In Air				
Room Temp.	080525-1	632	61	83
Room Temp.	080525-6	929	66	51
Room Temp.	080829-1	346	59	59
40 days 180°C	080530-1	592	58	33
40 days 180°C	080601-1	786	62	36
91 days 180°C	080526-1	760	62	40
91 days 180°C	080531-1	767	68	36
136 days 180°C	080712-1	197	45	26
136 days 180°C	080713-1	152	40	23
In Argon				
40 days 180°C	080801-1	68	21	20
91 days 180°C	080803-1	67	22	23
136 days 180°C	080802-1	225	27	27
136 days 180°C	080802-6	112	25	32

1.4.3. Thermite Powders Thermite powders consist of a mixture of aluminum flakes and cuprous oxide in a stoichiometric weight ratio of 11:89. Since the binding energies of the aluminum 2s and of the copper 3p subshells are almost identical, no spectra were recorded on the aluminum 2s photopeaks. Oxide thickness data were ascertained only through Auger line intensities. Figure 8 illustrates representative spectra for the different aged thermite powders.

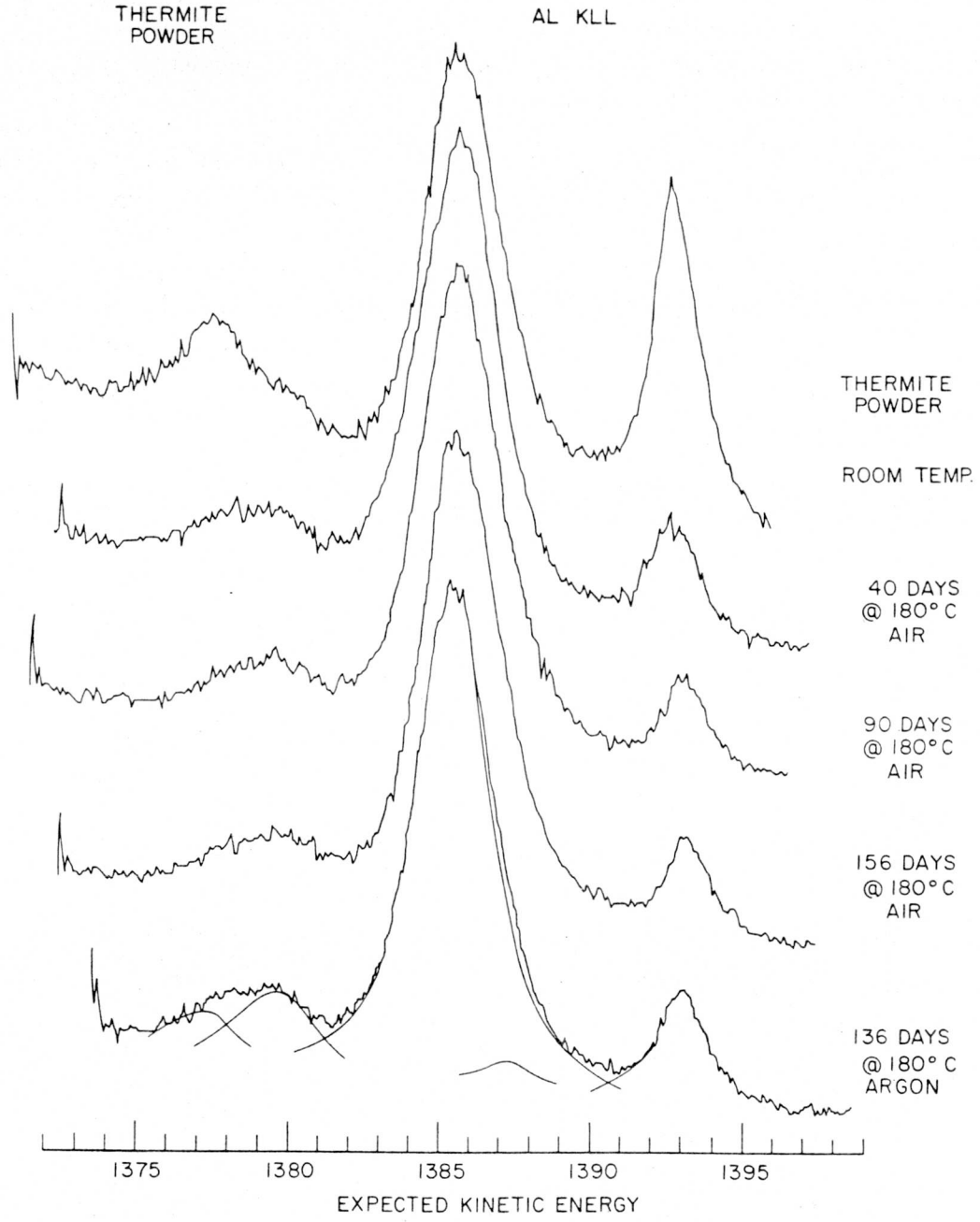

FIGURE 8 - Representative scans of aluminum K-$L_{2,3}L_{2,3}$ Auger peaks for aged thermite powders.

Oxide thicknesses were calculated using the peak areas obtained from the Auger lines and Eq. (7). The results of these calculations are summarized in Table 7. Comparison of the oxide data given in Tables 5 and 7 leads to the conclusion that the aluminum oxide thickness increases as a result of simply mixing the reactants to form the stoichiometric thermite powder. The oxide layer further thickens upon aging at 180°C in dry air, (d_O = 24Å) and upon aging in argon (d_O = 22Å). In both cases of aging, a larger increase in oxide thicknesses on aluminum can also be noted in the aged thermite powder mixtures compared to aged aluminum powdered material. Thus, it can be concluded that the increased oxide growth rate on aluminum in thermite powders is in great part the result of oxygen transfer from the cuprous oxide to the aluminum metal.

1.4.4. Thermite Pellets The pellets were obtained by a consolidation procedure of pressing the thermite powdered mixture in preheated, highly polished, graphite dies which were contained under an atmosphere of dry nitrogen [8]. The resulting pressing process gave cylindrical pellets of ∿6 mm in diameter and ∿2 mm in height. These samples were mounted directly in the XPS sample holder and inserted into the XPS spectrometer for analysis. A Teflon-coated razor blade was used for generating a fractured surface of a pellet. Oxide and carbon thicknesses were obtained, as before, by Eq. (7) and (9). Figure 9 illustrates representative scans of the aluminum K-$L_{2,3}L_{2,3}$ Auger transition of the aged thermite pellets. Table 8 summarizes the calculated carbon and oxide thickness data from the aged pellets.

Table 7 - SUMMARY OF MEASURED ALUMINUM OXIDE THICKNESS ON THERMITE POWDERS

Sample	Run No.	Intensity of Aluminum K-$L_{2,3}L_{2,3}$ Line I_O (counts-eV/sec)	Intensity of Aluminum K-$L_{2,3}L_{2,3}$ Line I_M (counts-eV/sec)	d_O (Å)
Air				
Room Temp.	080726-1	1340	669	10.0
Room Temp.	080729-1	1460	695	11.0
40 days 180°C	080724-1	1142	165	21.4
91 days 180°C	080725-1	1160	119	24.9
136 days 180°C	080725-1	774	88	23.8
136 days 180°C	080728-1	1102	127	23.7
Argon				
136 days 180°C	080806-1	1446	194	22.7
136 days 180°C	080806-10	276	35	22.1

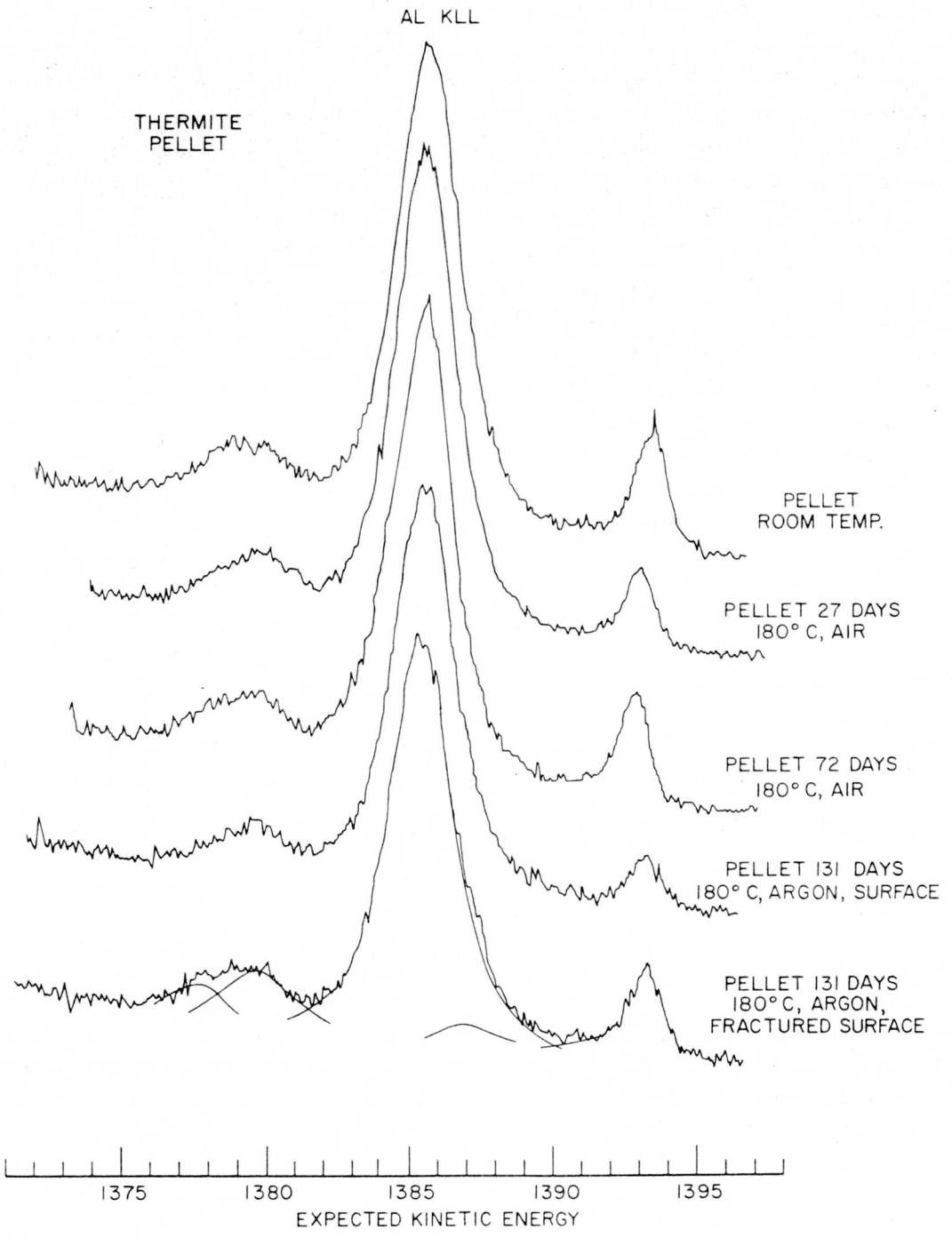

FIGURE 9 - Representative scans of aluminum K-$L_{2,3}L_{2,3}$ Auger transition peaks of aged thermite pellets.

Table 8 - SUMMARY OF MEASURED OXIDE AND CARBON THICKNESSES ON THERMITE PELLETS

Sample	Run No.	Intensity (counts-eV/sec): Intensity of Al K-$L_{2,3}L_{2,3}$ Auger Line I_O	Intensity (counts-eV/sec): Intensity of Al K-$L_{2,3}L_{2,3}$ Auger Line I_M	Intensity of Cu $2p_{3/2}$ / $I_{Cu\ 2p_{3/2}}$	I_C	$I_{Al\ K\text{-}LL} / I_{Cu\ 2p_{3/2}}$	d_O (in Å)	d_C (in Å)
Air/Surface								
Room Temp.	080801-1	1548	203	1098	160	1.59	22.4	11
27 days 60°C	080824-1	2185	211	787	249	3.06	25.5	18
27 days 180°C	080801-1	1392	121	613	101	2.47	25.7	13
27 days 180°C	080802-1	762	69	359	73	2.31	26.5	16
72 days 180°C	080731-1	1815	224	625	174	3.26	25.0	20
Air/Fractured Surface								
27 days 60°C	080824-8	637	73	1024	108	0.66	23.7	12
131 days 180°C	080815-1	511	60	1235	129	0.46	23.4	17
Argon Surface								
131 Days 180°C	080813-1	598	45	99	572	6.48	27.1	75

The effect of room temperature storage on oxide thicknesses of aluminum is shown in Figure 10. One will conclude that the oxide thickness is substantially larger following the consolidation procedure on the thermite powder. This thickness was calculated to be 22Å. Thus, in summary, the oxide increases in the following order: room temperature stored (9Å) <thermite powdered mixture (11Å) <consolidated thermite pellet (<22Å). Also, similar to the behavior of thermite powder, the oxide thickness reaches a constant thickness of 26Å on the pellet surface stored in air.

The total K-$L_{2,3}L_{2,3}$ aluminum intensity was divided by the copper $2p_{3/2}$ intensity in order to determine the possibility of surface diffusion in the pellet. Figure 11 illustrates the intensity ratio plotted as a function of the aging time. As can be determined from the plot, there is enrichment of aluminum on the pellet surface during the aging process.

1.5. Discussion of error

The major sources of error in determining oxide and carbon thicknesses are inherent in the variables of Eq. (1). As already mentioned, the photon flux was kept constant by means of a highly stabilized x-ray supply. The x-ray filament current was held at 5 mA, and the anode potential was kept at 10 kV. The rated stability of the supply is <.01% variation in the power output over one day of continuous operation and a much greater stability for a shorter duration. Although the variation in photon flux is directly proportional to variations in x-ray power, oftimes tungsten plating from the filament on the anode and/or x-ray window causes

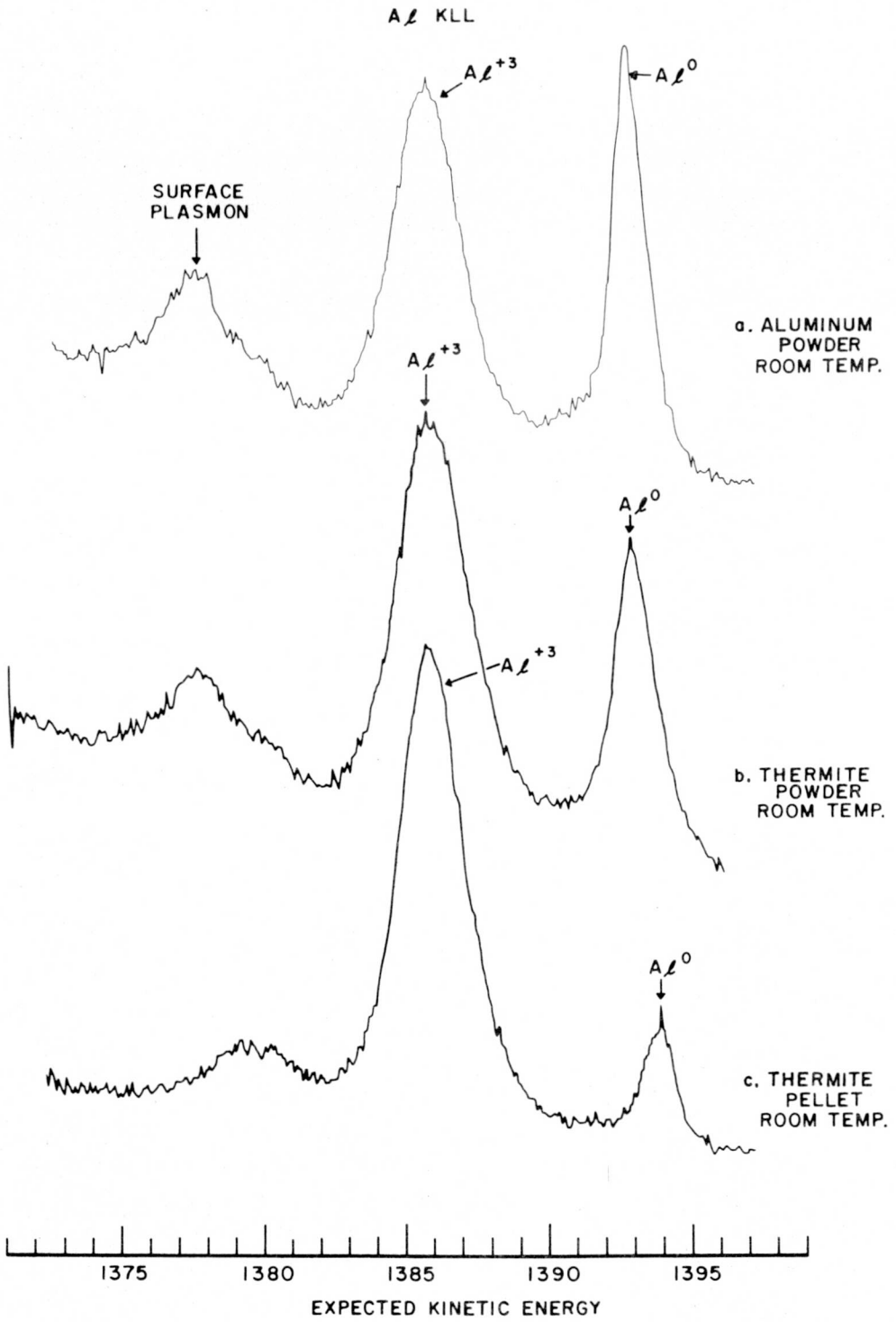

FIGURE 10 - Comparison of the aluminum K-$L_{2,3}L_{2,3}$ Auger peaks for room-temperature-aged (a) aluminum powder, (b) thermite powdered mixture, and (c) thermite pressed pellet.

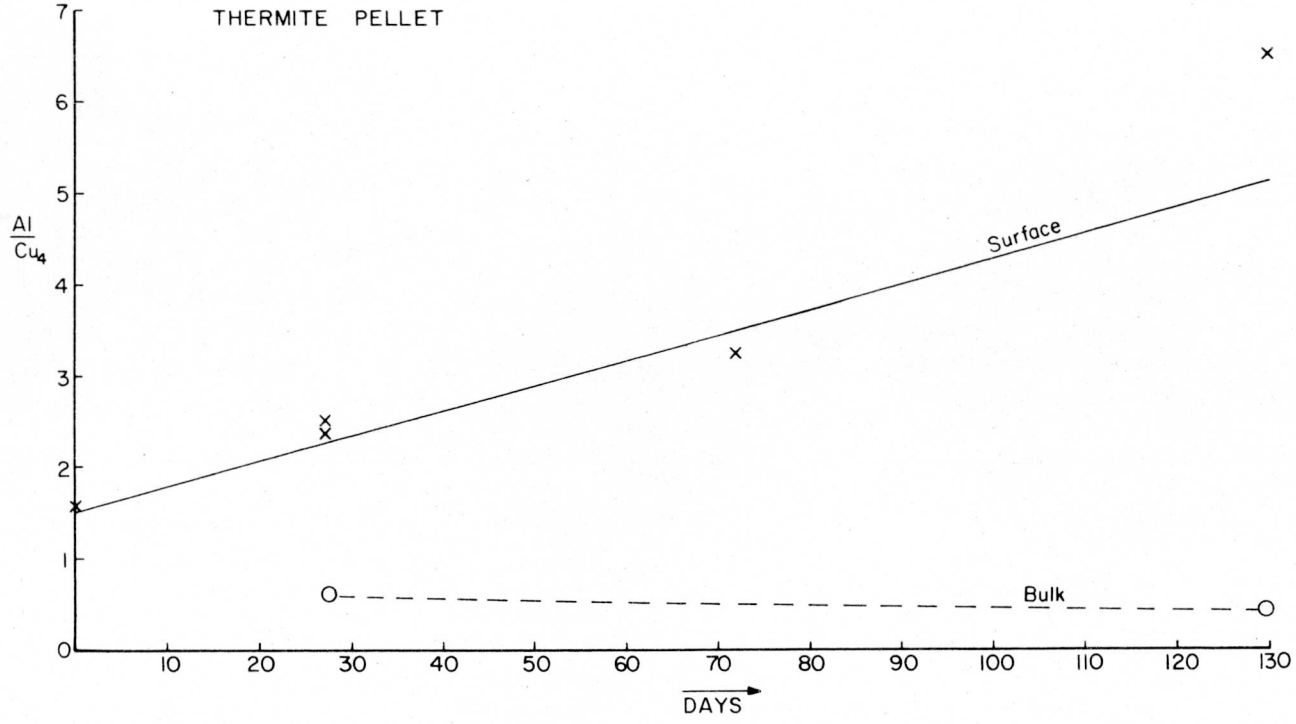

FIGURE 11 - Ratio of the aluminum K-$L_{2,3}L_{2,3}$ Auger intensity to the Cu $2p_{3/2}$ photoelectron intensity for the aged thermite pellets. Aging temperature of 180°C.

severe degradation in characteristic photon flux reaching the sample. In this study, the counting rate on Au $4f_{7/2}$ of an argon-ion-cleaned gold specimen was measured prior to, during, and following the thermite study. Counting rates on gold varied <5% during the entire study. The net counting rate on the Au $4f_{7/2}$ was 760 $\pm$ 15 counts/sec above background. The full width at half maximum for this line measured 1.2 eV. Also, to ensure that the flux remained constant during the study, the condition of the anode and window were checked immediately following the thermite analysis. No tungsten discoloration could be noted on either the anode or window.

Other variables in Eq. (1) are the spectrometer transmission function and the cross-section for photoionization. The spectrometer was set in a fixed analyzer transition mode of operation. In this mode, the analyzer is fixed for detecting 65 eV electrons, and the lens is varied in potential. All spectra were recorded in this mode of operation. For a particular level, the cross-section is constant and dependent only on the subshell excited and the photon source.

The remaining variables of Eq. (1) are the mean free path and sample area being analyzed. The use of the correct mean-free-path values can be the largest source of error in accurately determining oxide thickness. Mean-free-path values, λ, can be determined, however, only with great difficulty. As already mentioned, to keep within the scope of this study, literature values of λ were used. These varied in quoted confidence. At 95% confidence the quoted λ values deviated by as much as 20%.

Table 3 listed the I_o values measured for 5 x 5 mm^2 and 5 x 6 mm^2 specimens. For the limited amount of available data, a 25% increase in sample area corresponds to ~30% increase in intensity in I_o. Perhaps more interesting are the I_o^* values and their standard deviations which reflect the reproducibility of the maximum intensities observable from aluminum and aluminum oxide. For only five independent measurements, I_o^* was found to be 5722±514 for the Al K-LL Auger peak, a standard deviation of 8.9%.

Other variables to be considered are errors in estimating background, changes in angular detection, interface structure, and surface roughness. Each of these possible causes is addressed below.

The background observed with the standard materials, metal aluminum foil and the oxide grown on the foil, had a gradual sloping background, whereas the background observed with the powdered specimens showed a significant increase in signal strength as the kinetic energy decreased. The increased sloping background with the powdered specimens made the peak area more difficult to measure. Also, a contribution resulting from overlapping lines had to be considered in the determination of the oxide peak area in the K-LL aluminum spectra of mixed oxide/metal powdered specimens. This is illustrated in Figure 3, where the ^1S Auger state excited in the metal overlaps the ^1D excited in the oxide. A DuPont 310 Curve Resolver was used to measure the peak areas in this study. The error in measuring the areas of the same peak was less than 5% in these studies, even in cases of unusually large changes in background and in cases where there were extensive contributions from peak overlapping.

The equations used for measuring the oxide thicknesses assume continuous, layered, and homogeneous thin films. It has been shown by Ebel [9] that nearly all these deviations from the ideally flat, smooth, and homogeneous film structure can cause the observed discrepancies in d_o of Eq. (7). The d_o deviations were found to vary with analysis angular detection, where surface roughness was determined to be the major cause of the observable deviation. Clark et al. [10] also studied the angular dependence of homogeneous and inhomogeneous gold and polymer substrates and thin films. They noted that the intensity ratio of film/substrate was a function of the angle of incidence that the x-ray beam makes with the sample surface. In this study of oxide and carbon thicknesses, the angle of incidence was kept at 45°, and the surface roughness was assumed to be constant. This latter assumption is not unreasonable since the samples were all powdered specimens of flaked aluminum and of cuprous oxide with both having particle sizes of less than 10 μm [8]. These thermite samples can be assumed to be infinitely rough, therefore, with little deviation from specimen to specimen. Also already mentioned, the residual gas analysis spectra taken earlier on the same vacuum system showed hydrogen, water vapor, and carbon monoxide to be the major constituents at a pressure of 2 x 10^{-8} torr. A study done by Shiraki et al. [11] on the absorption of carbon monoxide on clean aluminum films found that both an Al-C type of bond and an Al-O type bond are formed. In our calculations it was assumed that the carbon layer is over the initial oxide formed. This need not be true for a freshly sputtered aluminum metal foil. Additionally, it was shown that the initial oxide growth on a clean aluminum surface is not stoichiometric

Al_2O_3 but can consist of suboxides [7,12]. Mean-free-path values could differ under these circumstances in intensity measurements used to correct for oxide and carbide growth; and, therefore cause additional error in d_o of Eq. (7).

2. Copper chemistry

2.1. Aged cuprous oxide

Figure 12 illustrates the Cu $2p_{3/2}$ and the Cu $L_3M_{4,5}M_{4,5}$ Auger spectra of (a) copper metal, (b) CuO, and (c) Cu_2O. These results agree with previously published literature data [13-16]. Figure 12 also illustrates the characteristic multiple excitation lines associated with the paramagnetic ion (Cu^{+2}, d^9) [17-20]. The broadness in the main photopeak noted at 0 eV relative kinetic energy is the result of spin exchange interactions observed during photoionization of cupric ions [17-18], and the broad photopeak cnetered at -8.5 relative energy is characteristic of the complementary shake-up electrons emitted during photoionization of cupric salts [19-20].

Figure 13 illustrates the Cu $2p_{3/2}$ and Cu $L_3M_{4,5}M_{4,5}$ Auger spectra for the stored Cu_2O specimens. Table 9 summarizes the

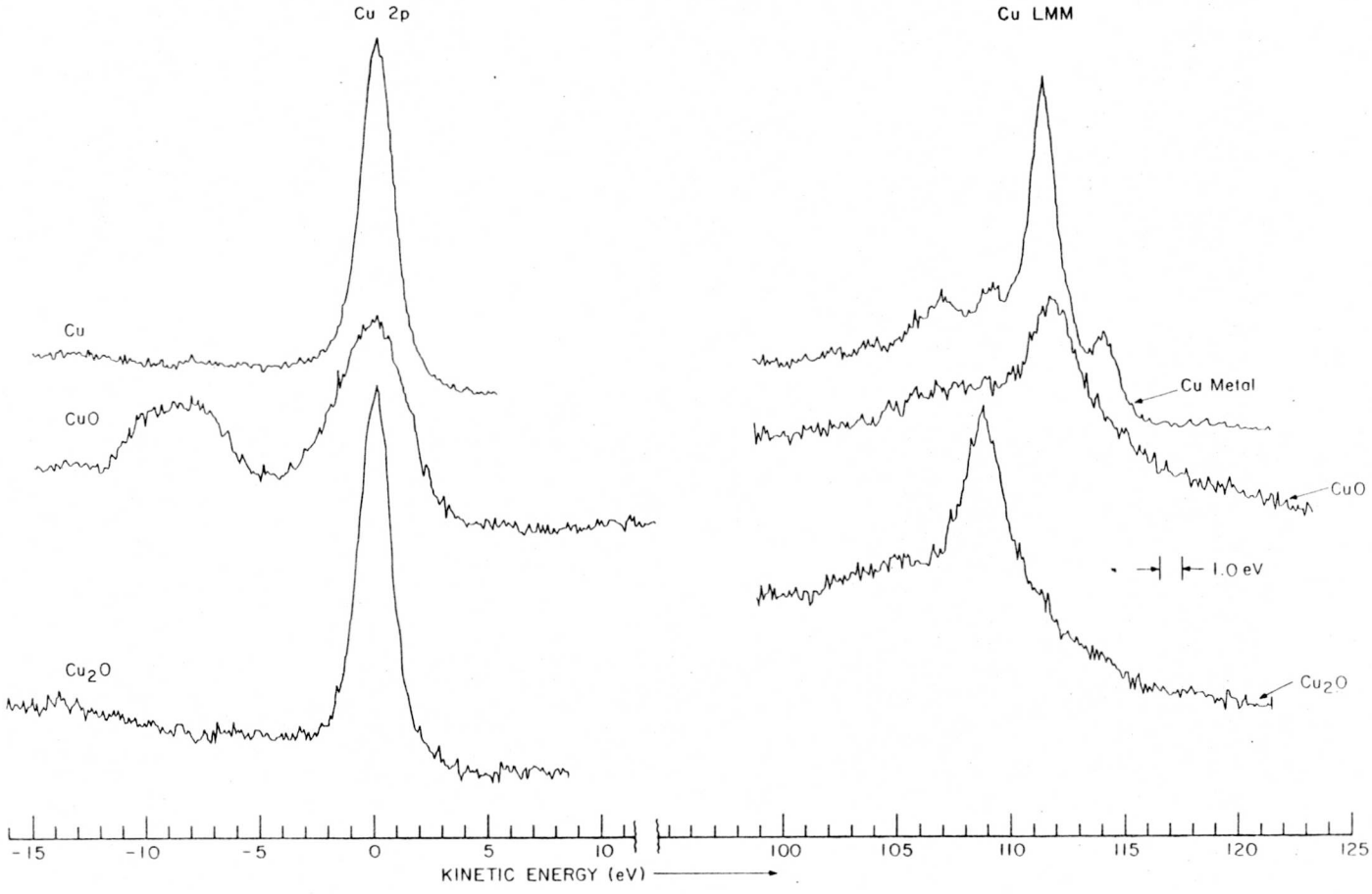

FIGURE 12 - The Cu $2p_{3/2}$ and the Cu $L_3M_{4,5}M_{4,5}$ Auger spectra of (a) copper metal, (b) CuO, and (c) Cu_2O.

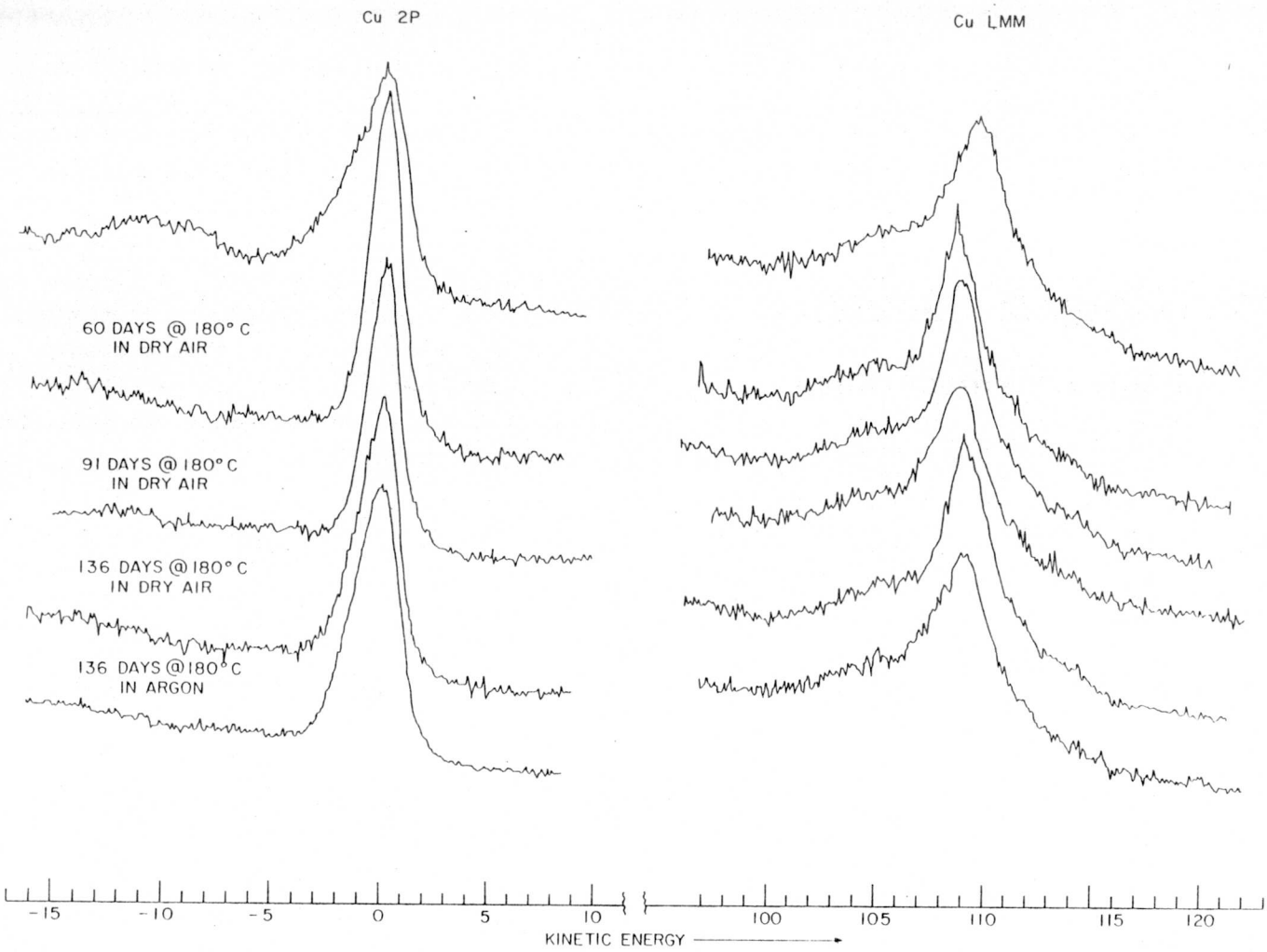

FIGURE 13 - The Cu $2p_{2/3}$ and the Cu $L_3M_{4,5}M_{4,5}$ Auger spectra of Cu_2O (a) stored at room temperature, (b) stored at 180°C in dry air for 60 days, (c) stored at 180°C in dry air for 91 days, (d) stored at 180°C in dry air for 136 days, and (e) stored at 180°C in argon for 136 days.

results illustrated in Figures 12 and 13. The following conclusions can be drawn from the above data on copper:

(1) The surface of the room-temperature-stored Cu_2O is contaminated with CuO. Deconvolution of both the Cu $2p_{3/2}$ and Cu $L_3M_{4,5}M_{4,5}$ Auger peaks indicates that the surface contains 35 $\pm$ 10% CuO.

(2) The surface cupric oxide is decomposed into Cu_2O when stored at 180°C in dry air for 40 days.

(3) Carbon and oxygen are reduced by heating to 180°C in air. The O 1s/Cu $2p_{3/2}$ ratio is reduced by $\sim$1/10 upon heating.

(4) As time of heating increases, the difference in kinetic energy between Cu $2p_{3/2}$ and the Cu Auger increases slightly from 108.8 eV to 109.2 eV. Since no CuO satellite could be observed in the specimens aged for 136 days, the observed peak broadening and shift were assumed to result from

Table 9 - SUMMARY OF HIGH RESOLUTION XPS AND AUGER DATA ON Cu_2O POWDERS

Compound	Binding Energy (eV)			Δ Kinetic Energy (eV)	Raw Intensity Ratio	
	Cu $2p_{3/2}$	Cu A	O 1s	(Cu 2p - Cu A)	C 1s / Cu $2p_{3/2}$	O 1s / Cu $2p_{3/2}$
Cu-metal (before sputtering)	933.0	-	-	-	-	-
Cu-metal (after sputtering)	933.4	917.5	-	111.4	-	-
Cu_2O	934.5	916.8	529.8 531.6 533.4	111.8	0.70	
Cu_2O (R.T. stored)	933.3	915.9	531.3 532.9	109.7	0.63	1.56 1.27
Cu_2O (40 days in air @ 180°C)	933.5	914.8	531.1 532.8	108.8	0.029	0.131 0.023
Cu_2O (91 days in air @ 180°C)	933.2	915.1	531.0 532.7	109.0	0.091	0.265 0.066
Cu_2O (91 days in air @ 180°C)	933.2	915.3	531.0 532.7	109.0	0.12	0.194 0.045
Cu_2O (136 days in air @ 180°C	933.3	915.4	531.1 532.8	109.2	0.044	0.181 ∿0.030
Cu_2O (136 days in air @ 180°C)	933.3	915.5	531.0 532.8	109.2	0.034	0.180 ∿0.060

the formation of copper metal. An estimate of <10 at. % metal formation on the surface can be made.

A surface chemisorbed oxide was measured at 533.5 eV binding energy. This oxide species is removed by heating. The nature of this oxide and how it is affected by aging will be studied in future examinations.

2.2. Thermite powders

Figure 14 illustrates the Cu $2p_{3/2}$ and Cu Auger for the thermite powders stored at room temperature and at 180°C. From these data, one will immediately note the doublet in the Cu $2p_{3/2}$ spectra of Figure 14(a) and thr broad Auger peak of Figure 14(b). Comparing these data to the data in Figures 12 and 13, one can conclude that

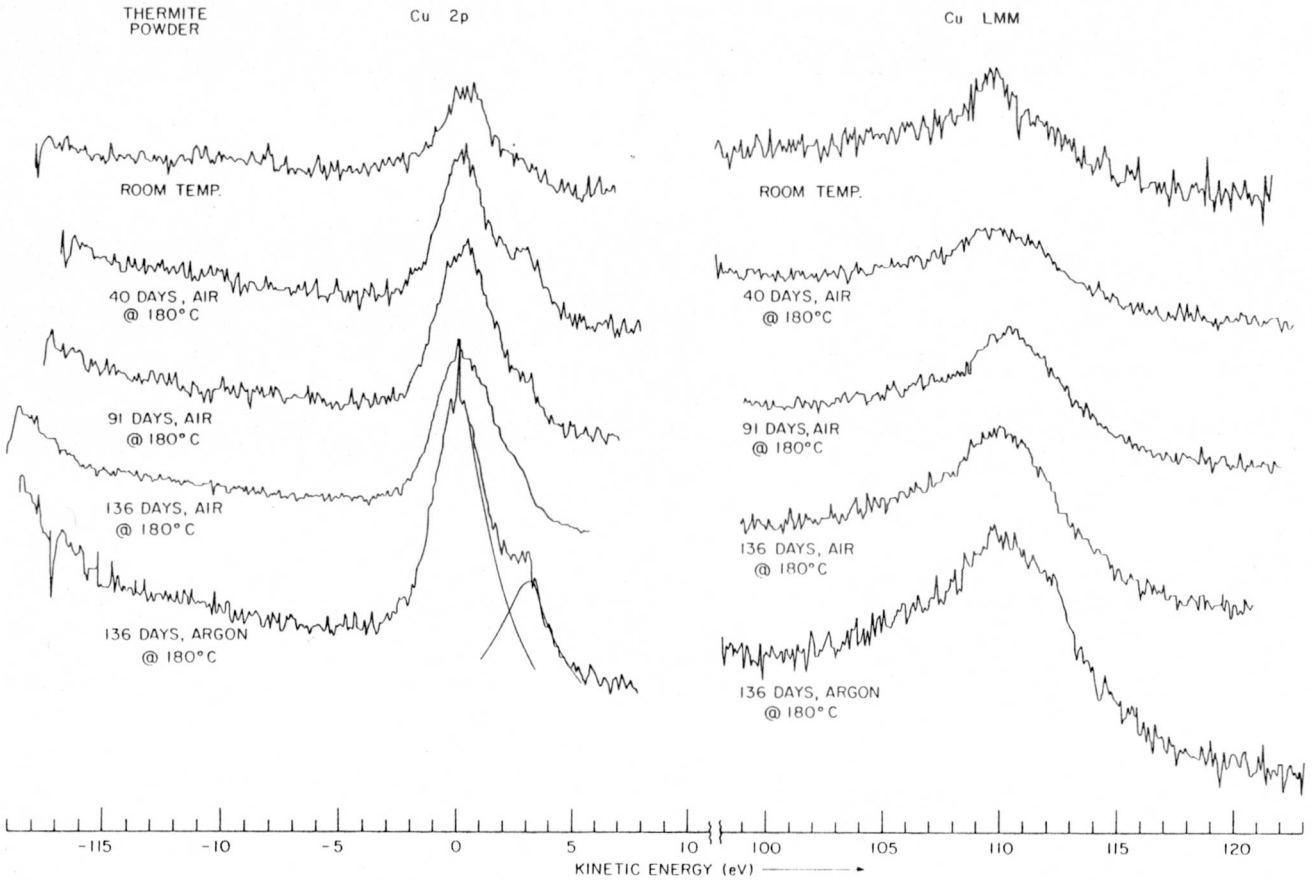

FIGURE 14 - The Cu $2p_{3/2}$ and Cu $L_3M_{4,5}M_{4,5}$ Auger spectra of thermite powder: (a) stored at toom temperature, (b) stored at 180°C in dry air for 40 days, (c) stored at 180°C in dry air for 91 days, (d) stored at 180°C in dry air for 136 days, and (e) stored at 180°C in argon for 136 days.

the copper chemistry in the thermite mixture has been altered via contact with the aluminum powder. The Cu $2p_{3/2}$ photopeak noted at 993.3 eV binding energy can be attributed to Cu_2O and the photopeak appearing at 930.0 eV is most probably "metallic like" in character (possibly an alloy of aluminum and copper). The true origin of this later photopeak still remains to be assigned.

2.3. Thermite pellets

Figure 15 illustrates the Cu $2p_{3/2}$ and the Cu Auger for the thermite pellets. It is interesting to note that the Cu $2p_{3/2}$ photopeak at 930.0 eV is absent. The spectra show that the surface of the room-temperature-aged pellets is Cu_2O contaminated with a small amount of CuO. Upon aging at a higher temperature of 180°C for 27 days, the surface of the pellet becomes enriched with CuO. At 72 days the CuO decreases.

3. Summary

XPS data were recorded on the Al 1s, Al 2s, Cu $2p_{3/2}$, and C 1s levels of the thermite components, aluminum metal flakes and cuprous oxide powder. High resolution AES scans were made on the Al K-$L_{2,3}L_{2,3}$

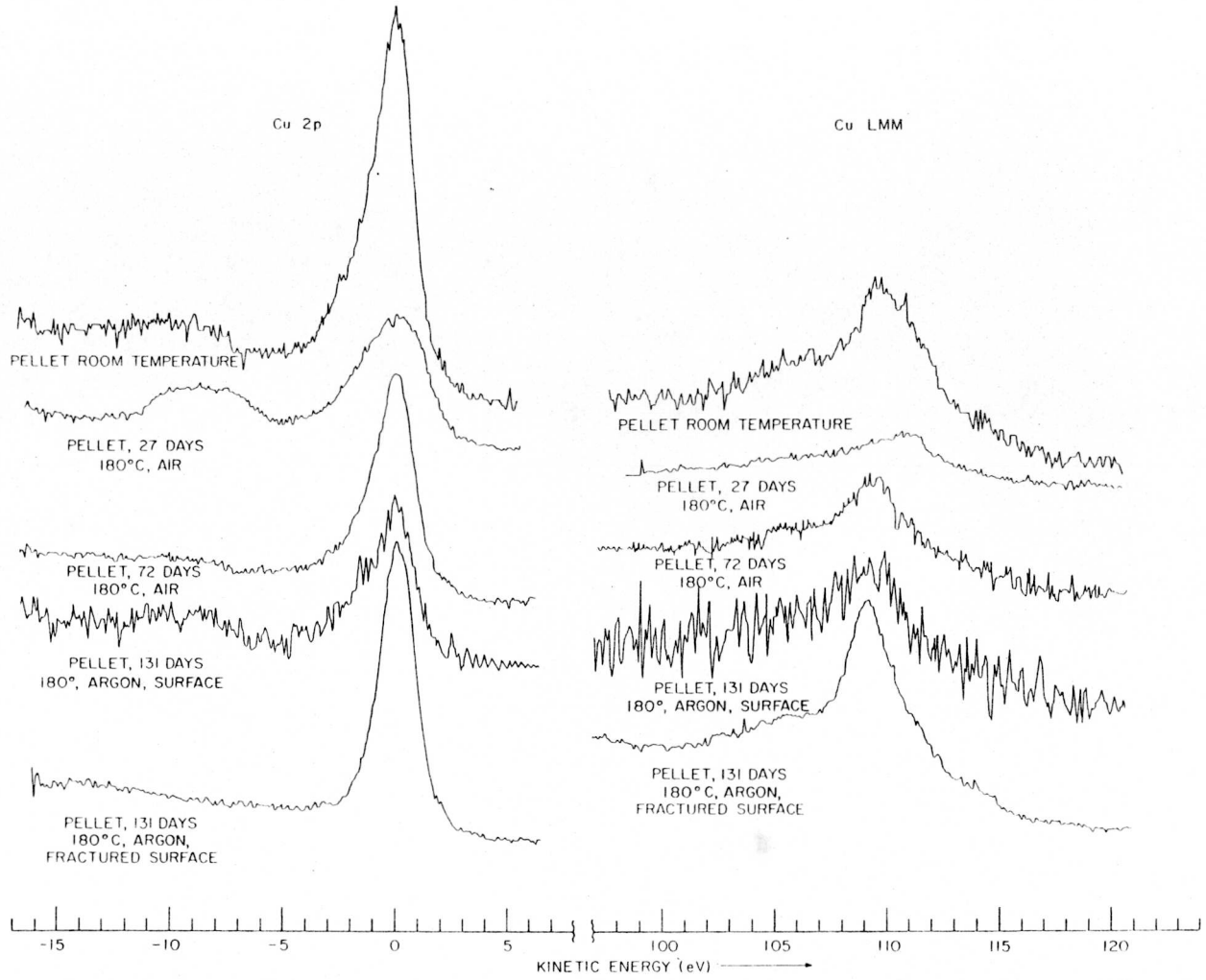

FIGURE 15 - The Cu $2p_{3/2}$ and Cu $L_3M_{4,5}M_{4,5}$ Auger spectra of thermite pressed pellet: (a) stored at room temperature, (b) stored at 180°C in dry air for 27 days, (c) stored at 180°C in dry air for 72 days, (d) stored at 180°C in argon for 131 days, and (e) fractured surface of (d).

and on the Cu $L_3M_{4,5}M_{4,5}$ transitions of the thermite components. XPS and AES data were also collected on the thermite blend and on the thermite consolidated pressed pellet. Equations relating the intensity of the photoelectron and Auger peaks to the thickness of the surface contaminants and/or reaction products were developed.

On the aluminum metal flake powders no change in surface oxide or surface carbon levels could be noted for specimens aged at room temperature in dry air. Surface oxide thicknesses of 9 ± 1Å were measured on the room-temperature-stored powdered aluminum. Upon an increase of storage temperature to 180°C and contact with dry air, the aluminum oxide thickness increased. At 40 days of storage, the oxide measured 13 ± 1Å. After 91 and 136 days the oxide remained constant at 13 ± 1Å. Carbon contaminant levels decreased upon storage at 180°C from 64Å for room-temperature-stored metal to 34Å for high-temperature-stored powder.

The largest oxide thicknesses calculated were 23 ± 1Å on aged thermite powders and

25±Å on aged pressed pellets; minimum carbon contamination measured ≤ 20Å on these aged samples. It is interesting to note that the aluminum oxide increases in the following order for room temperature aged specimens: aluminum metal powder (9Å) < thermite powder (11Å) < thermite pressed pellet (22Å).

Copper Auger and photoelectron data detected the presence of CuO on the surface of room-temperature-aged Cu_2O and noted the formation of metal on high-temperature-aged Cu_2O and aged thermite powder. A chemisorbed oxide was also noted on room-temperature-stored Cu_2O which decreased upon heating.

4. References

1. C. D. Wagner, Anal. Chem., 49, 1282 (1977).
2. A. Rengan, L. D. Haws, W. E. Moddeman, and P. S. Wang, Surface Studies on the Thermite Mixture of Al/CuO_2, I. Auger and X-Ray Photoelectron Results Using Si K_α X-Radiation, MLM-2751 (October 7, 1980).
3. F. P. Mertens, Surf. Sci., 71, 161 (1978).
4. T. A. Carlson and G. E. McGuire, J. Electron. Spectros. Relat. Phenom., 1/2, 121 (1974).
5. F. L. Battye, J. Liesegang, R. C. G. Leckey, and J. G. Jenkin, Phys. Lett., 49A, 155 (1974).
6. B. L. Henke, J. Phys. C., 4, 115 (1971).
7. S. A. Flodstrom, R. Z. Bachrach, R. S. Baner, and S. B. M. Hagstrom, Phys. Rev. Lett., 37, 1282 (1976).
8. L. D. Haws, M. D. Kelly, J. H. Mohler, and A. Latkin, "Consolidated Al/Cu_2O Thermites," presented at the 6th International Pyrotechnic Seminar, Estes Park, Colo., 17-21 July 1978, MLM-2531(OP).
9. M. F. Ebel, J. Electron Spectros. Relat. Phenom., 14, 287 (1978).
10. D. T. Clark, A. Dilks, D. Shuttleworth, and H. R. Thomas, J. Electron Spectros. Relat. Phenom., 14, 247 (1978).
11. Y. Shiraki, K. L. I. Kobayashi, and Y. Katayama, Surf. Sci., 77, 458 (1978).
12. K. L. I. Kobayaski, Y. Shiraki, and Y. Katayama, Surf. Sci., 77, 449 (1978).
13. T. Robert, M. Bartel, and G. Offergeld, Surf. Sci., 33, 123 (1972).
14. P. E. Larson, J. Electron Spectros. Relat. Phenom., 4, 213 (1974).
15. J. F. McGila and P. Weightman, J. Phys. C., 11, 643 (1978).
16. D. C. Frost, A. Ishitani, and C. A. McDowell, Mol. Phy., 24, 861 (1972).
17. C. S. Fadley and D. A. Shirley, Phys. Rev., A2, 1109 (1970).
18. C. S. Fadley, D. A. Shirley, A. J. Freeman, P. S. Bagus, and J. V. Mallow, Phys. Rev. Lett., 23, 1397 (1969).
19. T. A. Norakov, P. Prins, and D. A. Shirley (ed.), Electron Spectroscopy, North Holland Publ. Co., Amsterdam, 1972, p. 821.
20. A. Rosenewaig, G. K. Wertheim, and H. J. Guggenheimer, Phys. Rev. Lett., 27, 479 (1971).

5. Acknowledgement

The work at the University of Dayton was funded by a subcontract from Mound Facility.

Distribution

EXTERNAL

TIC, UC-4 (164)
H. N Hill, DOE Dayton Area Office
R. K. Flitcraft, Monsanto Research Corporation
D. J. Dahm, Monsanto Research Corporation, Dayton
R. Maute, Monsanto Research Corporation, Dayton
R. E. Keller, Monsanto Company, St. Louis
W. E. Koerner, Monsanto Company, St. Louis
J. P. Mieure, Monsanto Company, St. Louis
A. Rengan, University of Dayton (2)
T. A. Carlson, Oak Ridge National Laboratory, Oak Ridge, Tenn.
Monsanto Technical Reports Library, St. Louis

INTERNAL

R. T. Braun
H. S. Carden
W. T. Cave
R. J. DeSando
R. J. Finney
L. D. Haws (2)
C. W. Huntington
J. R. McClain
W. E. Moddeman (30)
H. L. Turner
R. E. Vallee
P. S. Wang (15)
H. A. Woltermann
Publications
Library (15)

Published by Information Services:
Marjorie F. Hauenstein, Editor